Journal of Marine Research, 53, 539–569, 1995

Dynamics of circulation of the Japan Sea

by Greg Holloway[1], Tessa Sou[1] and Michael Eby[1]

ABSTRACT

Including mean flow forcing due to eddy-topography interaction in a numerical model of the Japan Sea appears to improve defects identified in previous modelling studies. Characteristic western boundary current overshoot (by the East Korea Warm Current) is reduced or eliminated while a southward undercurrent brings colder, fresher water along the Korean coast. Cyclonic circulation in the north includes a strengthened Liman Current. A more nearly continuous Nearshore Branch follows the Honshu shelf break with northward-flowing undercurrent. Interannual variability persists under fixed (seasonally repeating or annual mean) external forcing.

1. Description

Bounded by Japan, Korea and Russia, the Japan Sea (or East Sea) is a region of great practical interest. A semi-enclosed "small ocean" (Ichiye, 1984), roughly 1600 km long by 900 km wide with depth exceeding 3700 m and with only shallow straits (Tsushima, Tsugaru, Soya, Mamiya) connecting to the China, Pacific and Okhotsk seas, the Japan Sea provides a natural "laboratory" for testing ideas about ocean circulation.

The upper layer is cooler and fresher to the north and west, with seasonal occurrence of sea ice. Correspondingly, the upper layer is warmer and more saline to the south and east. Below about 400 m, water properties are nearly homogenous in the Japan Sea Proper Water. High oxygen in the colder regions extends to great depth, indicating convective exchange. Higher oxygen is found also in warmer regions beneath the warm, saline Tsushima water. Intermediate water (East Sea Intermediate Water of Uda (1935) or Kim *et al.* (1991) is marked by salinity minima in some locations.

Overall circulation is locally driven by winds, thermal and freshwater forcing and by inflow at Tsushima Strait with outflow at Tsugaru and Soya Straits (Fig. 1). Tides are weak in the Japan Sea (Kang *et al.,* 1991). Extending from 35N past 50N, the Japan Sea experiences significant variation of Coriolis parameter. A western boundary current, the East Korea Warm Current (EKWC) flows northward from Tsushima Strait to a confluence with the southward-flowing Liman Current (LC, also called

[1] Joint Program for Ocean Dynamics, Institute of Ocean Sciences, Sidney, B.C., V8L 4B2, Canada.

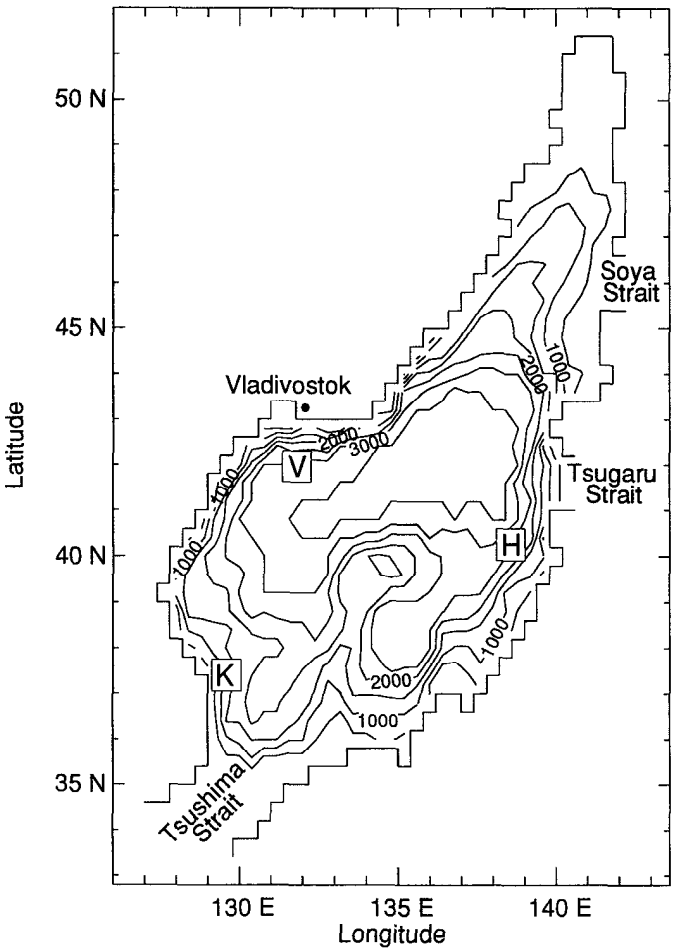

Figure 1. (a) Model geometry on 44 km grid, showing bottom topography and open straits (Tsushima, Tsugaru, Soya). Points K, V and H are marked for reference in the text. (b) A schematic of surface circulation is shown after Uda (1935).

North Korea Cold Current). Another branch of the inflow follows more nearly the shelf edge along Honshu, and is termed the Nearshore Branch (NB). Meanders and branching form seasonally in the inflow region (Kawabe, 1982). The NB flows northward to Tsugaru Strait where it is joined by the separated western boundary currents (EKCC and LC) which have flowed eastward along a meandering polar front. Some flow exits through Tsugaru Strait. Some flow continues northward to Soya Strait, where a further portion exits. Remaining flow closes a northern cyclonic gyre, reforming the LC. In subsurface flow, low salinity water of northern origin is seen to underthrust the EKCC and is found along the Korean coast nearly to Tsushima Strait.

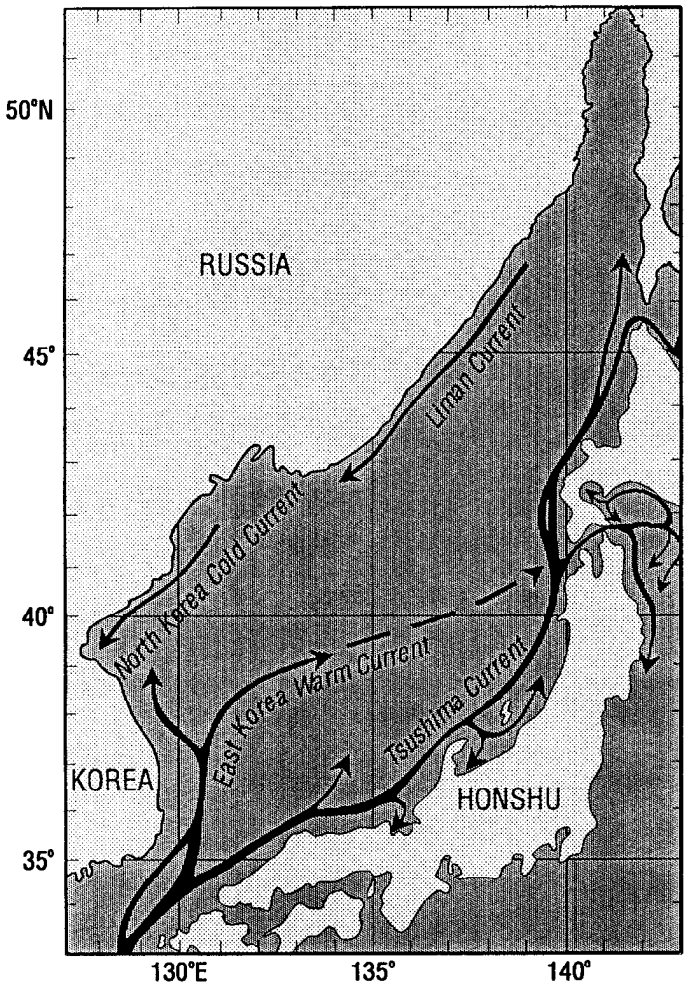

Figure 1. (Continued)

A wealth of observational, theoretical and numerical modelling studies have been conducted in the Japan Sea. Theory and numerical modelling, seen in Kawabe (1982), Yoon (1982a,b,c), Sekine (1986, 1991), Kang (1988), Seung and Kim (1989), Seung (1992), Seung and Nam (1992), and Seung and Kim (1993, hereafter SK) have attempted to sort out the different effects of forcings, of basin geometry, and of variation of Coriolis parameter. The recent study by SK employed high resolution, realistic forcing and realistic geometry. Despite realistic modelling, problems remain. Separation of the EKCC tends to occur too far north. The NB often seems underdeveloped while the LC is underdeveloped or reversed (as Sekine (1986, 1991)). Modelled subsurface currents are weak and of questionable direction relative to limited observations.

2. Motivation

We are motivated in part by the outstanding issues identified in earlier modelling studies. We are concerned about a possible systematic defect in our understanding of ocean physics, i.e. that eddies too small to resolve adequately (if at all) may interact with the shape of bottom topography to exert a powerful driving force on oceans. That force, termed topographic stress ("topostress"), is entirely absent or may be grossly misrepresented by ocean models. Holloway (1992) proposed possible parameterization which was refined for global ocean modelling by Eby and Holloway (1994a, hereafter EH) and used by Alvarez *et al.* (1994) in a study of circulation in the western Mediterranean. Similarities between the Mediterranean and Japan Seas suggest the present study.

Our aim here is not so much to make the "best" (most realistic) model of the Japan Sea, but more to clarify issues of ocean physics that must arise for other, more realistic models (e.g. employing more specific, presumably more accurate, surface forcing datasets).

During the course of this investigation, we observed interannual variability under seasonal (periodic) forcing. To clarify the nature of variability, we applied also steady (annual mean) forcing with both fine and coarser (hence more viscous) resolution. Under steady forcing on both fine and coarser grids, modelled flow exhibited spontaneous, aperiodic vacillations, not reported from earlier modelling studies. These phenomena also are discussed below.

3. Numerical model

The model used for this study is the Modular Ocean Model (MOM, Pacanowski *et al.,* 1991), after the original formulation by Bryan (1969). This is very nearly the model used also by SK. We have employed Euler angle rotation on the sphere (Eby and Holloway, 1994b) to place a computational grid with nearly equidistant vertices at 0.2° spacing (roughly 22 km). Vertical discretization consists of 25 levels from 25 m to 3780 m. Grid resolution is similar to that of SK. We've studied a number of cases at lateral grid spacing 0.4° with 25 levels, these cases motivated by computational economy over longer integrations and to compare dependence upon grid resolution. We have also replaced centered differencing in tracer (temperature and salinity) equations with a flux-corrected transport scheme developed by Gerdes *et al.* (1991) to minimize artificial diffusion.

Open straits include Tsushima, Tsugaru and Soya, while coastal boundaries include the west coasts of Honshu and Hokkaido and a portion of Sakhalin Island which is joined to the Asian continent. We impose inflow through Tsushima Strait ranging from zero to 2 Sv (10^6 m^3/s). The inflow is divided into outflow at Tsugaru and Soya Straits in the fractions ¾ and ¼ respectively. Rather than invoking open boundary conditions (as SK), we have included reservoirs outside the Tsushima and Tsugaru-Soya Straits, with outer boundary conditions on the reservoirs satisfying

periodic re-entrance. Within the reservoirs, temperature and salinity relax toward observed properties at the inflow to Tsushima Strait and the Coriolis parameter is remapped. Wind forcing is from monthly Hellerman and Rosenstein (1983, hereafter HR) while surface heat and freshwater forcing are implied by relaxing (on 10 day timescale) model temperature and salinity to the monthly and seasonal Levitus (1982) atlas. [SK have employed locally estimated winds from Na *et al.* (1992) while imposing (on approximately 5.6 hour timescale) surface temperature and salinity supplied from Japan Oceanographic Data Center (JODC, 1978). Visual comparison between the windstress interpolated from HR and that of Na *et al.* (1992) suggests they are broadly similar over most months, though differing in detail. Likewise the temperature and salinity from Levitus atlas broadly suggest the fields from JODC as shown by SK.] We use constant vertical viscosity of 10^{-4} m^2/s and horizontal viscosities of 10^3 and 2×10^3 m^2/s on the fine and coarse grids, respectively. No explicit diffusivity is assigned for the tracer fields. Initial conditions consisted of temperature and salinity fields given at all depths by horizontally averaged, depth-dependent Levitus data, with initial velocity fields at rest.

4. Representation of topostress

Following EH, we have introduced a simple representation of topostress. An approximate maximum entropy ("unprejudiced") flow field is calculated from a transport streamfunction $\Psi = -fL^2H$ where f is Coriolis parameter, L is a topostress length parameter and H is the depth of fluid. This defines a depth-independent velocity $\mathbf{u}^*$ given by $\mathbf{u}^*H = \mathbf{z} \times \nabla\Psi$. Where the eddy viscous tendency $A_m\nabla^2\mathbf{u}$ occurs in the model momentum equation, one writes $A_m\nabla^2(\mathbf{u} - \mathbf{u}^*)$ so that the eddy tendency is directed not toward a state of mean rest ($\mathbf{u} = 0$) but toward the higher entropy configuration $\mathbf{u} = \mathbf{u}^*$. L is a poorly known eddy parameter, plausibly related (Holloway, 1992) to scales somewhat shorter than a dominant eddy vorticity length scale. In their global calculations, EH assigned L to vary from 12 km at the equator to 3 km at the pole. In the Mediterranean, Alvarez *et al.* (1994) specified a constant $L =$ 4 km as giving "good" results. Noting that $L = 0$ restores a model to conventional usage, the question becomes a matter of parameter estimation. We examine choices for constant L ranging over $0 \leq L \leq 8$ km.

5. Mean circulation without topostress

First we seek to characterize the mean (i.e., time-averaged) flow without topostress (i.e., $L = 0$) under different combinations of imposed forcings by wind, thermal and freshwater, and assigned inflow at Tsushima Strait. We then compare results including topostress (nonzero L).

Before making extensive comparisons, we've sought to determine the effect of grid resolution upon the mean flow. Two runs were made as nearly identically as possible,

one on 44 km grid, one on 22 km grid with horizontal viscosity halved from its coarse grid value. With respect to mean flow variables (20 year average), effects of the different resolutions were slight. Both the northern cyclonic gyre and southern anticyclonic gyre were slightly stronger, with slightly narrower, swifter western boundary currents, on the 22 km grid. The latitude of confluence of EKWC and LC was insensitive to different resolutions of 22 and 44 km. Some differences were seen along Honshu where flows tended to be weaker and more variable. For economy and based upon relatively weak sensitivity to resolution, extensive tests reported in the following sections used the 44 km grid.

a. Influence of seasonality. In the experiments discussed in this paper, flows commenced from the endstate of 100 year integration under monthly wind, and seasonal thermal and freshwater forcing, with 1.5 Sv inflow at Tsushima. Further integrations were performed, in most cases over a 30 year period, after which time systematic transients were small (measured by such statistics as extrema of transport streamfunction or domain integrated kinetic energy). Although interannual variability persisted under both seasonal and steady forcing, statistics appeared to achieve quasistationarity. (Longer term drift was still occurring with respect to basin-wide depth distribution of temperature and salinity.)

We have sought to examine how important is seasonality of forcing with respect to the long term mean ocean state. The seasonally forced model was driven by monthly HR windstress with surface relaxation of temperature and salinity to monthly and seasonal Levitus values. Annual mean forcing used the annual-averaged windstress with surface relaxation of temperature and salinity to annual-averaged Levitus values.

An overall impression (Fig. 2) is that time-averaged features under seasonal forcing are not very different from time-averaged flow under steady (annual mean) forcing—for which the flow remains variable, as discussed in Section 7 (below). Although the seasonally forced case exhibits a somewhat stronger, more extensive northern gyre, it appears that rectification of the seasonal forcing is not a very strong consideration for these model runs. This may be a model defect from inadequate representation of seasonal convection.

For the several experiments described below, we retain full seasonality of windstress and buoyancy forcing.

b. Effects of local wind forcing. We omit wind forcing while retaining both the inflow forcing and the surface buoyancy forcing. Comparing the outcome (Fig. 3a) with a case of full forcing (Fig. 2a), one observes that wind plays a significant role maintaining the northern cyclonic gyre. Wind contributes to a stronger anticyclonic recirculation in a southern gyre, strengthening the EKWC by about 30%. With or

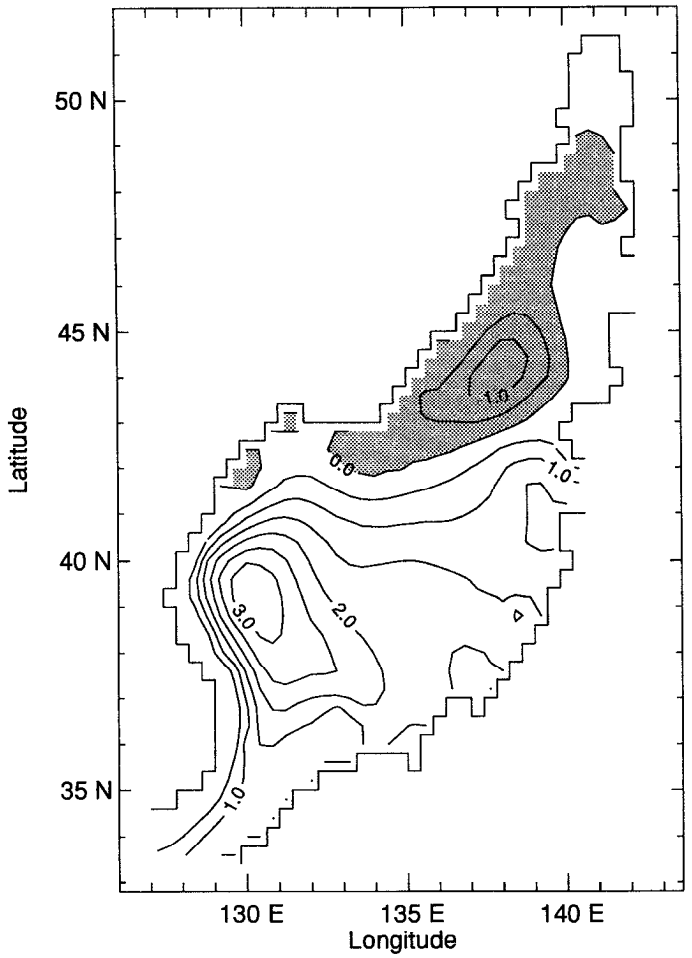

Figure 2. Time-averaged transport streamfunction (a) under seasonally-varying forcing and (b) under annual mean (steady) forcing. Units are Sverdrups (10^6 m^3/s.)

without wind, inflow from Tsushima Strait forms an EKWC which does not separate until above 42N.

Separation can be difficult to define because of a region of confused weak model flow off Vladivostok. In some model cases the EKWC may detach from the coast near 41N, or even at lower latitude. What is important though is confluence of the EKWC with the LC. In most model cases this confluence does not occur until east of Vladivostok. (Upper ocean velocity maps, showed later, indicate that the dominant confluence of modelled flow occurs near 42N, 134E.) In reality, the mean confluence occurs nearer 38N to 39N.

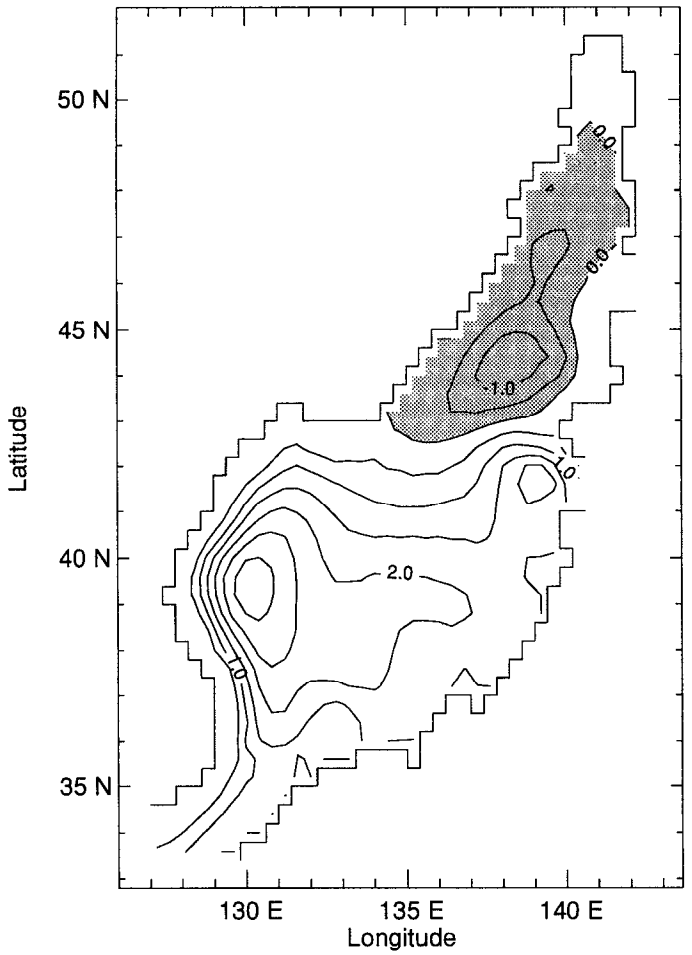

Figure 2. (Continued)

The HR windstress used here differs from the windstress of Na *et al.* (1992) used by SK, and may account for stronger penetration of the LC in results of SK.

With or without wind, there is little suggestion of a NB along Honshu. Differences in temperature and salinity fields are relatively slight.

c. *Effects of surface buoyancy forcing (heat and freshwater).* We omit surface forcing of the temperature and salinity fields (restoring is turned off at the surface) while retaining inflow forcing and wind forcing. Differences are small compared with full forcing, suggesting that buoyancy forcing is not so significant relative to wind. The northern gyre is weakened, indicating that buoyancy loss contributes to the cyclonic gyre. The southern (anticyclonic) gyre also is slightly weakened when buoyancy

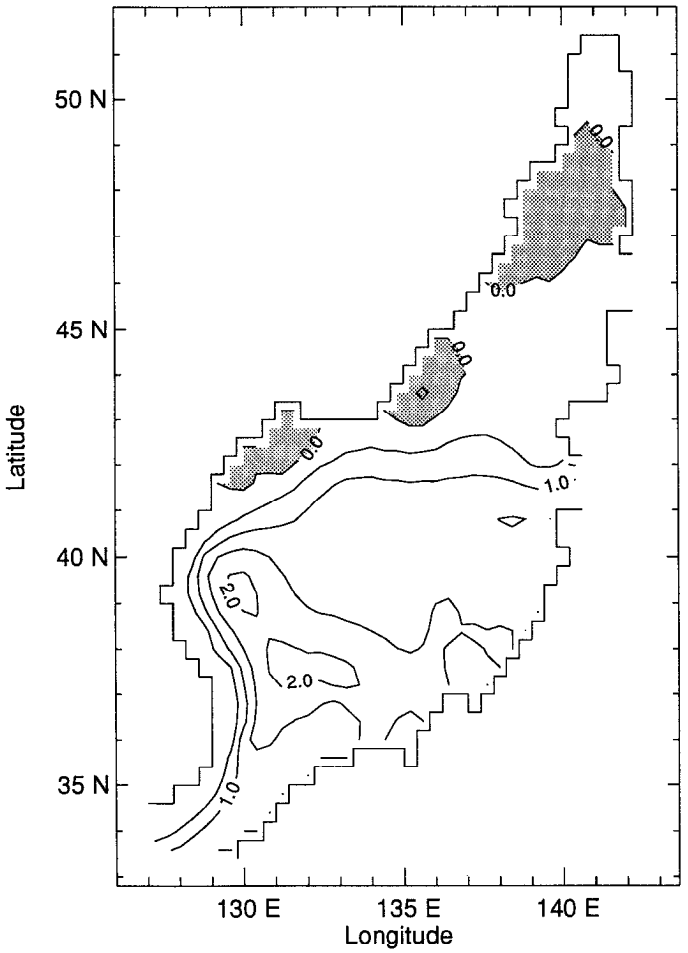

Figure 3. Time-averaged transport streamfunction under seasonal forcing (a) omitting wind-stress and (b) omitting surface buoyancy forcing.

forcing is omitted. The presence or absence of buoyancy forcing has little discernable effect on the separation of the EKWC or on the NB. In the absence of surface forcing of temperature and salinity, these fields must gradually become more homogenous, approaching values specified at Tsushima inflow. Streamfunction pattern (Fig. 3b) retains features due to wind and inflow forcing with only modest differences from full forcing (Fig. 2a).

A caution should be mentioned. Although surface buoyancy forcing appears not to play a dominant role, internal vertical buoyancy fluxes (from mixing parameterization) may be influential. This has been considered by Seung and Kim (1989) and Seung (1992) in context of a layered quasigeostrophic model with parameterized inter-layer buoyancy flux. The result showed an impact upon upper-layer streamfunc-

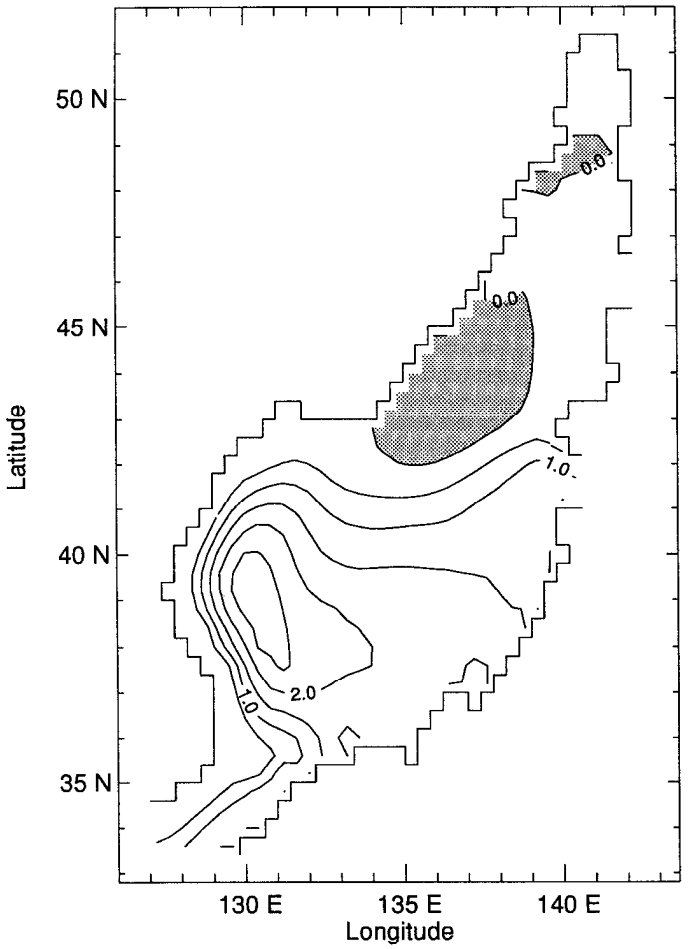

Figure 3. (Continued)

tion separation, albeit in idealized geometry under quasigeostrophic dynamics. Although we've not specifically pursued this concern in the present study, it is one of several suggestions that refinements to mixing and convection parameterizations may be important to overall model skill.

d. Forcing by assigned inflow through Tsushima Strait. We remove both wind and surface buoyancy forcings. Flow is entirely driven by specifying 1.5 Sv inflow at Tsushima Strait. In the southern portion, results are similar to the case of full forcing as inflow tends to follow the Korean coast in a broad EKWC, yielding a recirculating anticyclonic gyre. There is less cyclonic gyre in the north and no significant NB along Honshu (Fig. 4a).

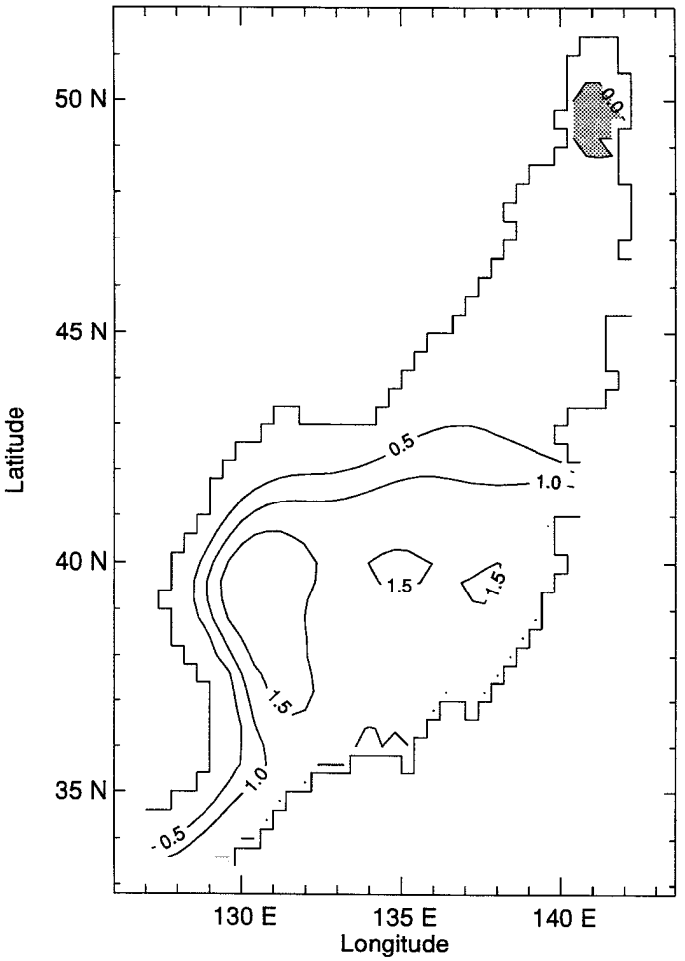

Figure 4. Time-averaged transport streamfunction forced only by specified inflow (1.5 Sv), without windstress or surface buoyancy forcing; (a) with latitudinally-varying Coriolis and (b) with Coriolis fixed at 40N.

e. Dependence on variation of Coriolis parameter. Why do models so tend to channel inflow along the western margin as EKWC? Yoon (1982c) and Kang (1988) suggested that the variation of Coriolis parameter may be important for this. We examine this hypothesis by setting Coriolis to a constant value (40N) throughout the model domain. For the case of forcing only by assigned inflow, the result is a broadening of the northward flow without clear western intensification, similar to the two layer results showed by Kang (1988) but unlike the barotropic model result of Yoon (1982c). The EKWC and NB become indistinct portions of the northward flow, while exhibiting greater northward penetration along Honshu (Fig. 4b). Latitude of separation of the EKWC is indistinct due to the breadth of the flow, but is not

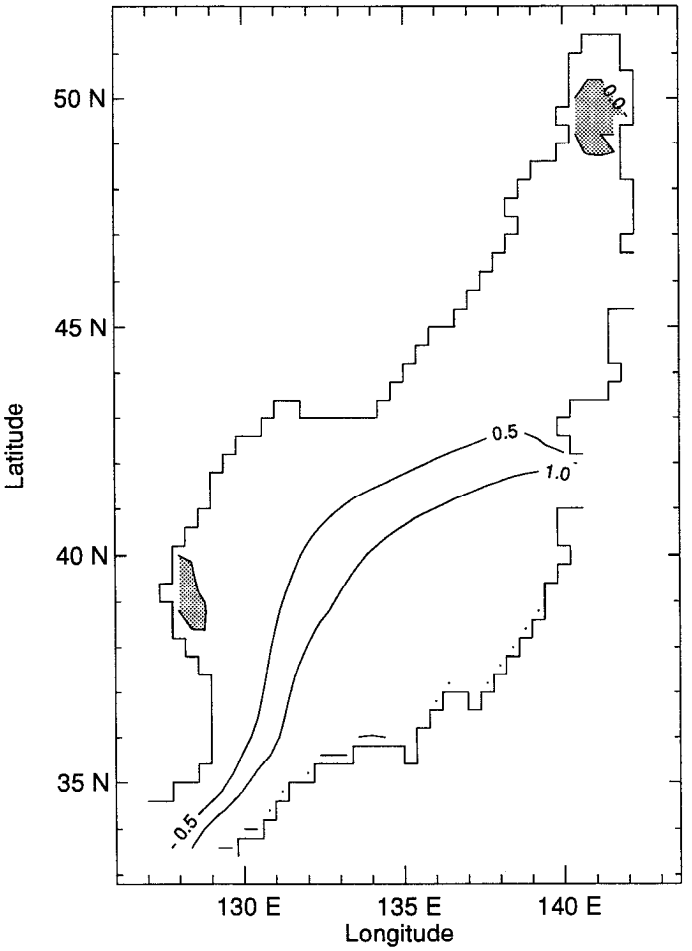

Figure 4. (Continued)

discernably different from the separation latitude with full variation of Coriolis. A cyclonic gyre in the north was nearly absent under only inflow forcing, and remains nearly absent with constant Coriolis.

When local forcing by wind and buoyancy is present with constant Coriolis, lack of beta-effect Sverdrup balance permits stronger gyres (in excess of 5 Sv in the southern gyre, not shown) without western intensification.

f. Summary without topostress. For conventional modelling without topostress (i.e., $L = 0$) remote forcing by inflow at Tsushima Strait tends to dominate circulation over the southern Japan Sea, supplying an EKWC that flows northward well past its realistic confluence latitude. Local wind forcing dominates a cyclonic gyre in the

north while surface buoyancy forcing (in the manner we've applied it) seems least effective. Deficiencies include the false separation of the EKWC, a northern cyclonic gyre and a NB that are underdeveloped, and absence of southeastward flow beneath the EKWC.

These defects are not unique to the present model formulation. The upper ocean layered model of Cherniawsky and Holloway (1993), including mechanisms for entraining momentum, heat and salt among layers, results in a Japan Sea dominated by anticyclonic circulation. Indeed the problems (perhaps linked) of western boundary current overshoot and of underdeveloped high latitude cyclonic gyre are chronic to model applications elsewhere (e.g., Bryan and Holland, 1989; Ezer and Mellor, 1992; Beckmann *et al.*, 1993).

6. Inclusion of topostress

We have attempted (above) to make a brief survey of ways that time-averaged circulation depends upon external forcings. With this background we now ask how much the results depend upon uncertain model physics, in particular the role of topostress. Results discussed above have been for cases without topostress, i.e., when $L = 0$. We include topostress by considering $L = 4$, 6 and 8 km. Runs were performed on the 44 km grid by continuing integration from the end of 100 years ($L = 0$) under full seasonal forcing. Runs were then continued for 30 years, with averaging over the last 20 years.

Effects of topostress are seen in Figure 5, showing mean transport streamfunction for $L = 4$ and 6 km to compare with $L = 0$ (Fig. 2a). With increasing L, the cyclonic gyre in the north intensifies and grows while the anticyclonic gyre weakens. These plots of transport streamfunction give an exaggerated impression because an important effect of topostress is to induce substantial flow throughout the water column. Historically we have supposed deep waters to be moving only weakly, and therefore view streamfunction as a convenient map of near-surface flow. The theory underlying topostress as well as direct observations in many areas of the world are indicating substantial mean deep flows which often may be opposed to surface flow.

To see the depth-dependence of flow, Figure 6 shows mean velocity maps at 75 m and 720 m depth from cases $L = 0$, 4, 6 and 8 km. With $L = 0$ flow at 75 m resembles the streamfunction seen in Figure 2a. Confluence of the EKWC with the LC occurs east of Vladivostok. Deeper flow (720 m) is weak and ambiguous off Korea.

With $L = 4$ km, flow at 75 m shows EKWC-LC confluence occurring south from Vladivostok, near 41N. This is still some hundreds of km north of a more realistic confluence, a defect that could be due in part to errors in HR windstress. The LC is strengthened and a NB can be traced from Tsushima to Tsugaru. At 720 m, a deep extension of the LC penetrates to nearly Tsushima Strait. Southeastward mean flow off Korea with amplitudes of about 2 cm/s agrees with current meter observations of Lie *et al.* (1989) and with deep float observation by Nan-niti *et al.* (1966). This

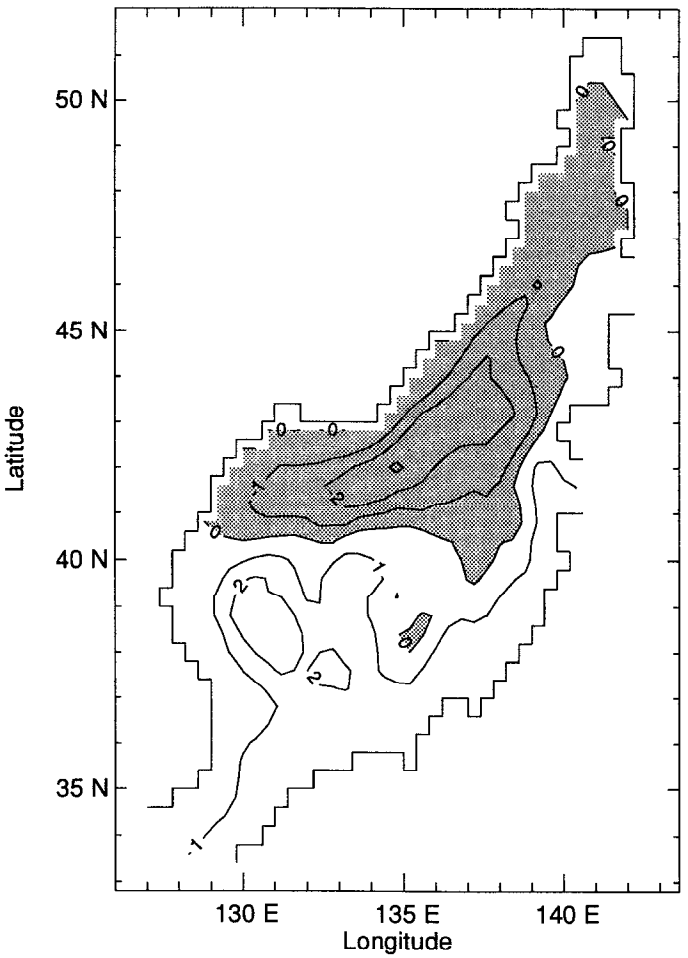

Figure 5. Time-averaged transport streamfunction under seasonally-varying forcing and topostress parameter (a) L = 4 km and (b) L = 6 km.

important feature is inferred also from hydrography by Kim *et al.* (1991) who compare it with the deep western boundary known in the North Atlantic.

With L = 6 km, flow at 75 m shows penetration of LC water to near 38N. Recall that these figures show time-averaged flow whereas actual penetration varies seasonally (Lie and Byun, 1985). An anticyclonic core, centered at about 136E, 39N occurs with L = 0 and with L = 4 and 6 km. This warm lens, somewhat north from the Ulleung Islands, is recovered also in model results of SK. The NB is well developed, as is the northern cyclonic gyre. At 720 m, flow patterns seen with L = 4 km are further strengthened. Southeastward flow off Korea has amplitudes near 4 cm/s.

Determination of L is not yet well understood. This is a topic of on-going research, the supposition being that the L reflects the higher wavenumber portion of an eddy

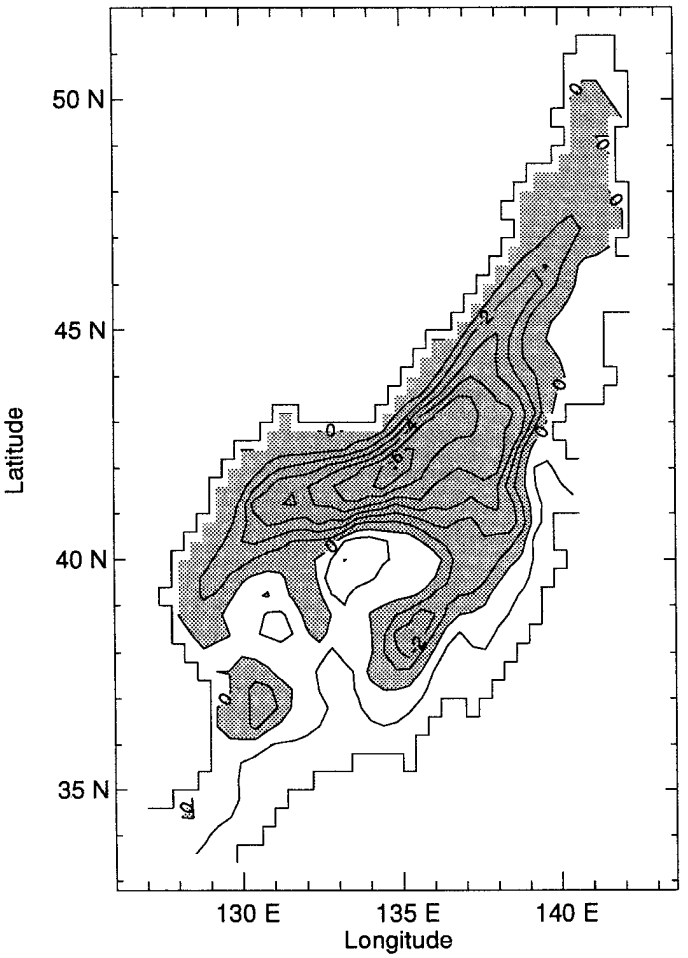

Figure 5. (Continued)

vorticity spectrum. L is an uncertain eddy parameter, not unlike usual eddy viscosity. Previously Alvarez *et al.* (1994) used $L = 4$ km in a study of the western Mediterranean, while EH used L ranging from 3 km at pole to 12 km at equator in a global ocean model. To extend the present sensitivity study, we show also flow at 75 m and 720 m with $L = 8$ km. At 75 m the EKWC has been displaced entirely offshore while broad southward flow dominates the Korean coast. Deeper flow is similar in pattern to $L = 6$ km results, but amplitude is greater. For the wind, surface buoyancy and inflow forcing used, and for the grid resolution and other model parameters used, it appears that 8 km is too large.

Different flow fields resulting from the different L have consequences in patterns of temperature and salinity. Near the surface these patterns are constrained by

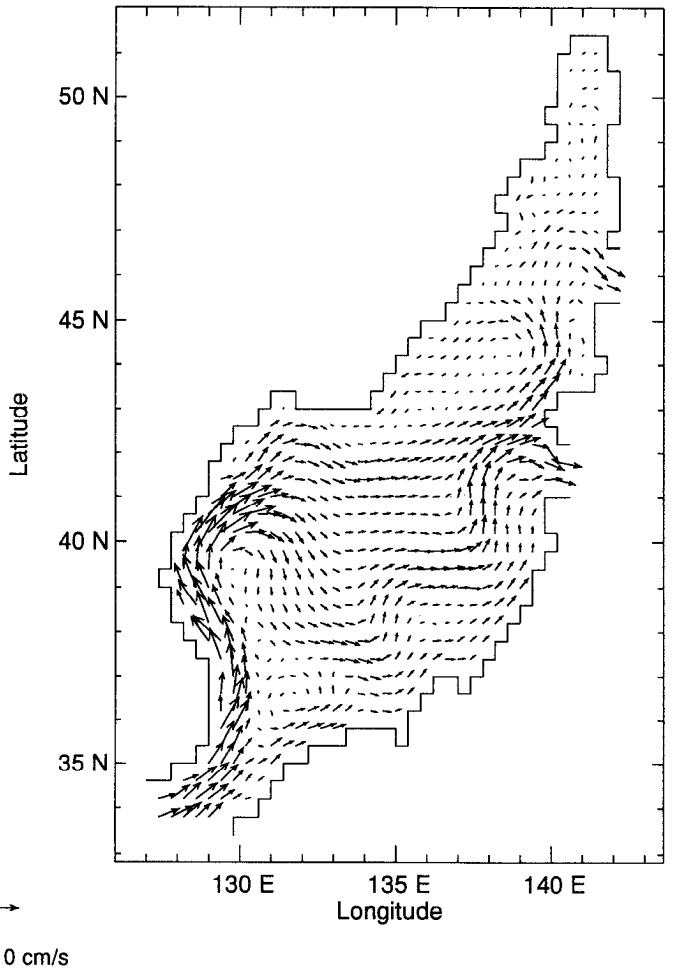

Figure 6. Time-averaged velocity fields at 75 m with (a) $L = 0$, (b) $L = 4$ km, (c) $L = 6$ km, (d) $L = 8$ km and at 720 m with (e) $L = 0$, (f) $L = 4$ km, (g) $L = 6$ km, (h) $L = 8$ km.

relaxation to remain "near" Levitus values. Differences become more evident below the surface layer. In Table 1 we compare differences of temperature and salinity between three locations (marked on Fig. 1):

K: a point off Korea near 37N, 130E

V: a point off Vladivostok near 42N, 132E,

H: a point off northern Honshu near 40N, 138E.

Comparisons are made at 100 m and 200 m for $L = 0$, 4 and 6 km with results listed in Table 1.

At 100 m, results from $L = 4$ km are not significantly different from $L = 0$, while at 200 m, already $L = 4$ km has impacts. All along Korea the water is colder at 200 m,

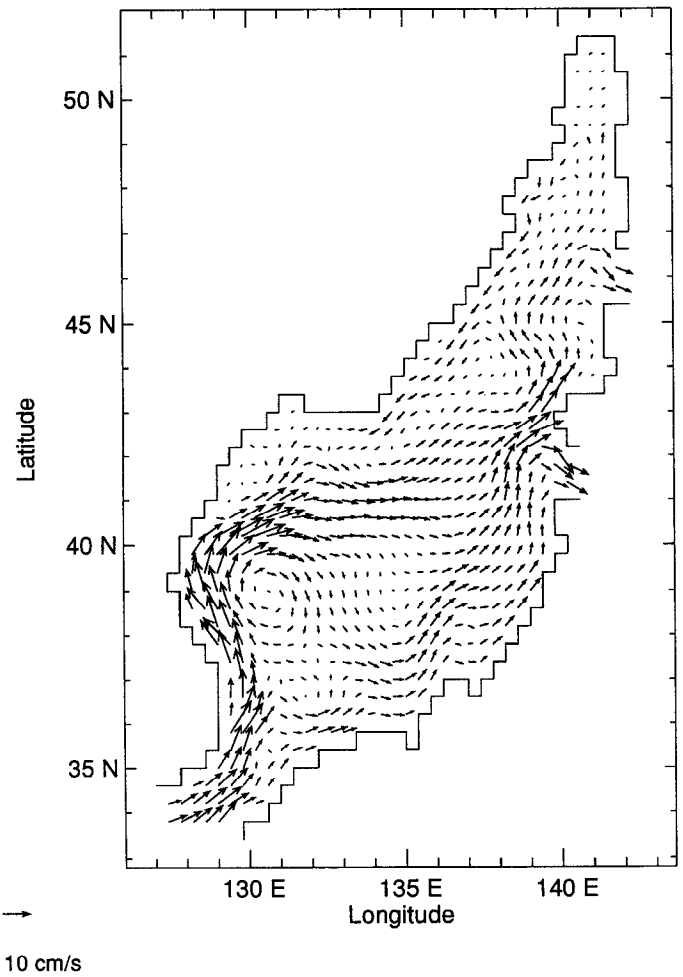

Figure 6b. L = 4 cm at 75 m.

Table 1. Temperature differences T(K-V), T(K-H) in °C and salinity differences S(K-V), S(K-H) in PSU are listed, where differences are between points K, V and H marked on Figure 1.

	100 m				200 m			
L	T(K-V)	T(K-H)	S(K-V)	S(K-H)	T(K-V)	T(K-H)	S(K-V)	S(K-H)
0	9.3	5.3	.35	.25	1.9	−.9	.07	.07
4 km	9.9	5.3	.43	.31	.5	−3.3	.06	.01
6 km	7.2	1.5	.31	.16	−.5	−4.9	.03	−.03

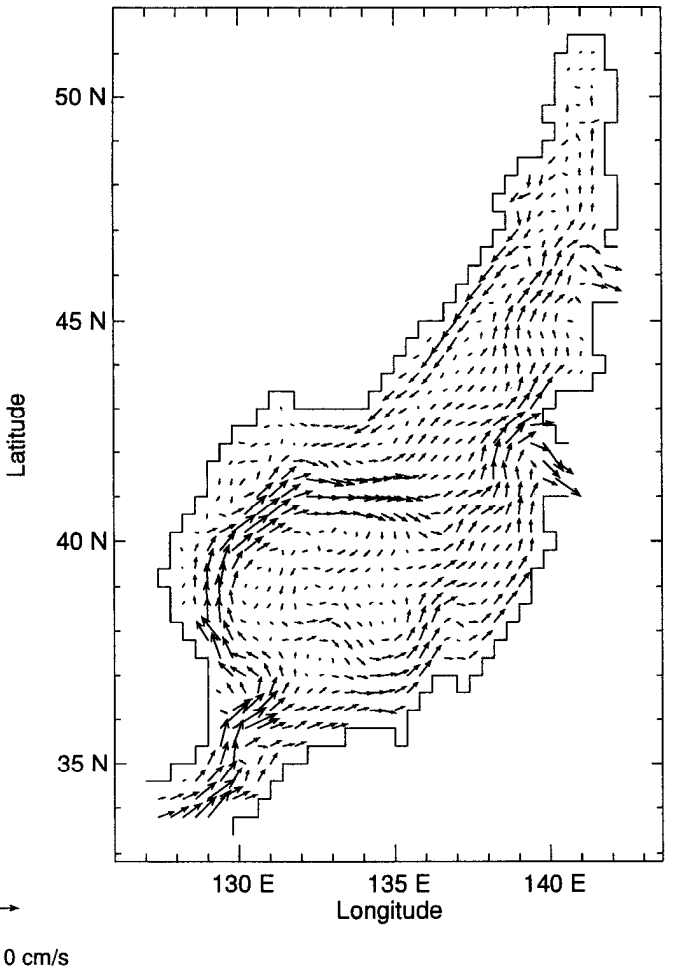

Figure 6c. L = 6 km at 75 m.

and the difference K-V is reduced. The more striking effect with L = 4 km is seen in the K-H difference where K is 3.3°C colder than H (vs. 0.9°C with L = 0). Somewhat lower salinity at K with somewhat increased salinity at H has lessened the K-H difference.

With L = 6 km, effects are seen at 100 m as well as 300 m. Colder water along Korea and warmer water along Honshu reduce the temperature differences K-V and K-H, especially the K-H difference. K-H salinity difference is reduced as well. At 200 m, effects are more pronounced. Temperature difference K-V has reversed sign to K colder than V. (Comparing temperatures at a fixed depth horizon is sometimes confused by differences in vertical movement.) Temperature at K is 4.9°C colder than at H, a difference which has increased by 4°C compared with L = 0. Salinity

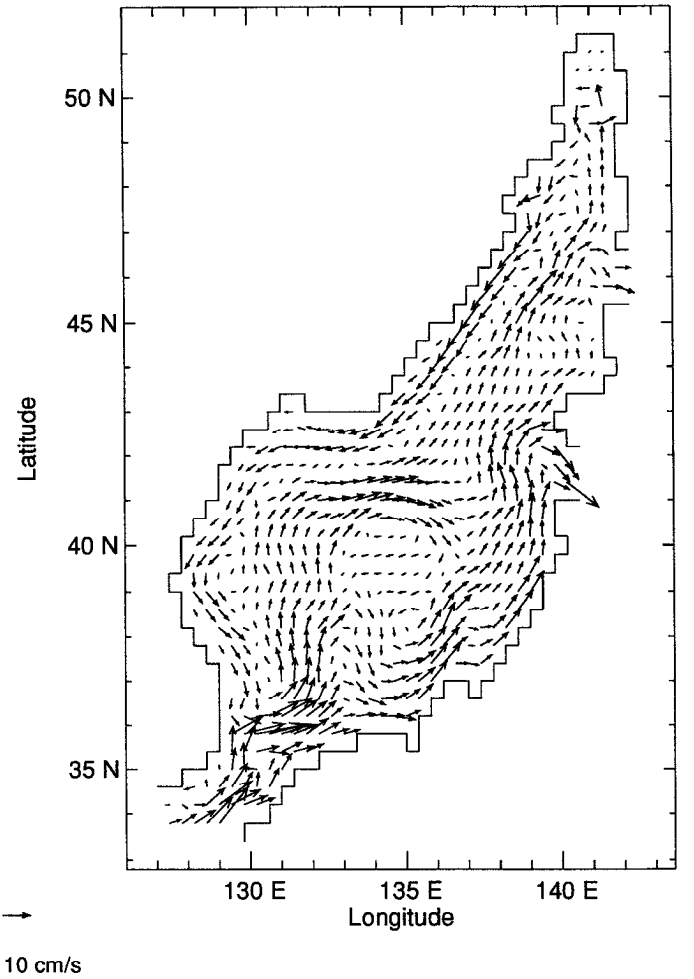

Figure 6d. L = 8 km at 75 m.

differences are seen, in particular reversing the sense of the K-H difference such that K is less saline than H, opposite to the case with $L = 0$.

Precise numerical values listed in Table 1 should not be given too much attention. The spatial patterns of these differences are complex, and different numerical values can be obtained by seemingly slight alterations. However, the sense of some of the differences listed in Table 1 is seen in individual plots. Figure 7 shows the difference field, seen in potential temperature and in salinity at 100 m, for the case L = 6 km minus the case $L = 0$. The effect of including topographic stress ($L \neq 0$) is most expressed by colder, fresher water along the Korean coast and somewhat more saline water along Honshu.

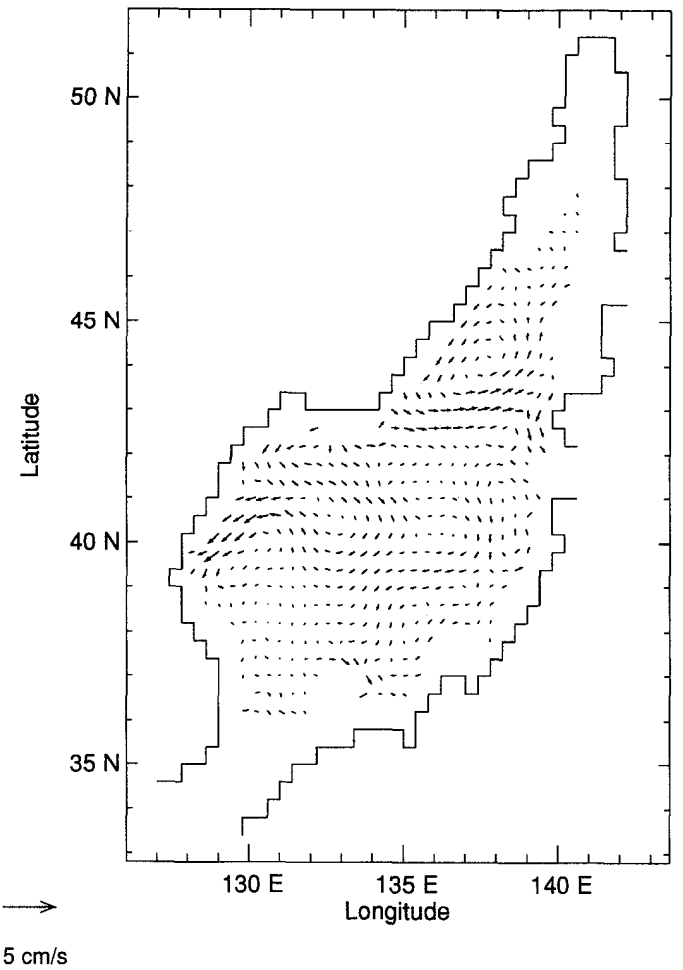

Figure 6e. $L = 0$ at 720 m.

7. Interannual variability

In the foregoing investigation, a repeating seasonal cycle was impressed in the forcing. We noticed model response showing persistent low-frequency (interannual) variability even after 100 year integration. This behavior was not identified in a similar model study by Seung and Kim (1993) but is discussed from observations by Toba *et al.* (1982) who attribute interannual variability to year-to-year variation of external forcing. We extended our investigation by applying steady (annual mean) forcing. This leads to enhanced low frequency variability. It appears that observed interannual variability in the Japan Sea may be partly internally generated within the Japan Sea, as well as by external forcing such as sea level differences between East China Sea and Tsugaru.

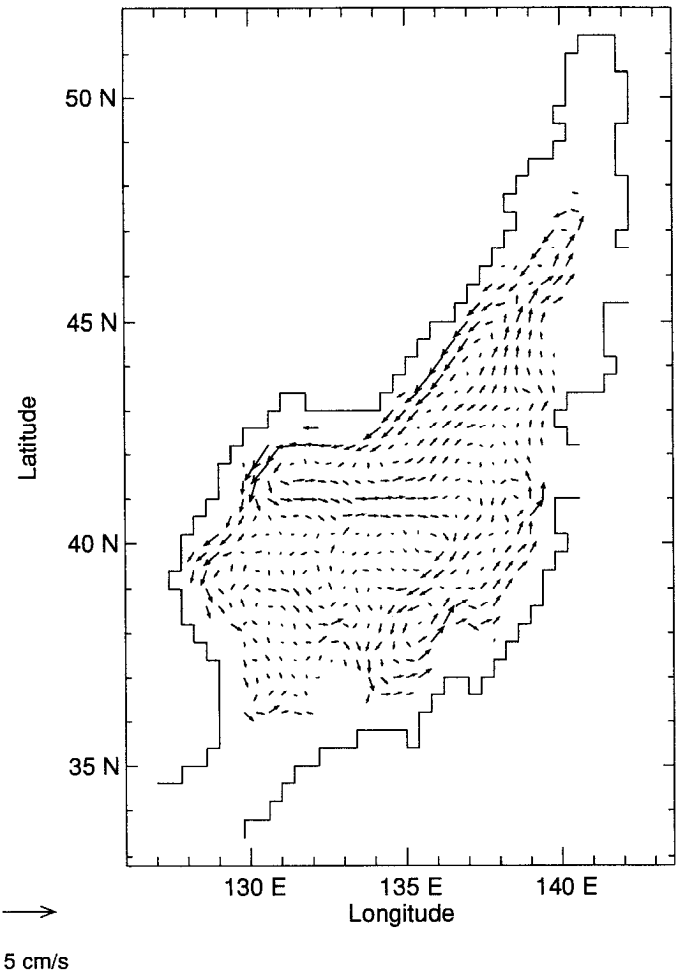

Figure 6f. L = 4 km at 720 m.

Modelled flow vacillates between two regimes. In one regime, flow from Tsushima follows the Korean coast then leaves the Russian coast and travels along 43N to exit at Tsugaru Strait (Fig. 8a). This is associated with a minimum of basin-integrated kinetic energy. In the other regime, associated with a maximum kinetic energy, water separates off the Russian coast, loops back toward Noto Peninsula and travels along Honshu before exiting through Tsugaru Strait (Fig. 1b). This regime has fresher, cooler water upper layers in the eastern portion of the Japan Sea. Changes in transport at location 40N, 138E can be compared to Toba *et al.* (1982) observation that baroclinic transport shows year-to-year fluctuations up to 0.4 Sv. We observe total transport fluctuations by more than 0.6 Sv. under steady forcing. These results

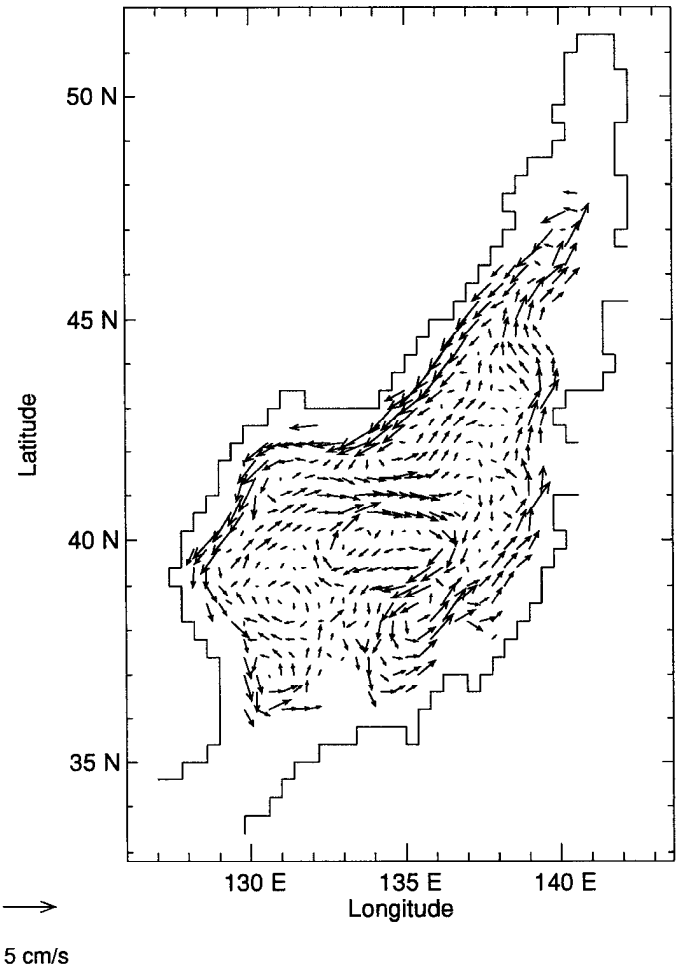

Figure 6g. L = 6 km at 720 m.

suggests that internally generated interannual variability may account for the observed variability even in the absence of externally forced fluctuations.

We have made a preliminary survey of the sensitivity of this variability to model resolution, to different external forcing, to variation of Coriolis parameter, to internal physical parameters, and to aspects of numerical method. Comparing results on the 22 km and 44 km grids, we find the variability persists on the coarser grid despite higher viscosity. Utilizing the coarser grid, we examined sensitivity to the following:

1) dependence upon surface forcing (surface buoyancy, wind stress)
2) dependence upon forcing by assigned throughflow,
3) dependence upon variation of Coriolis parameter,

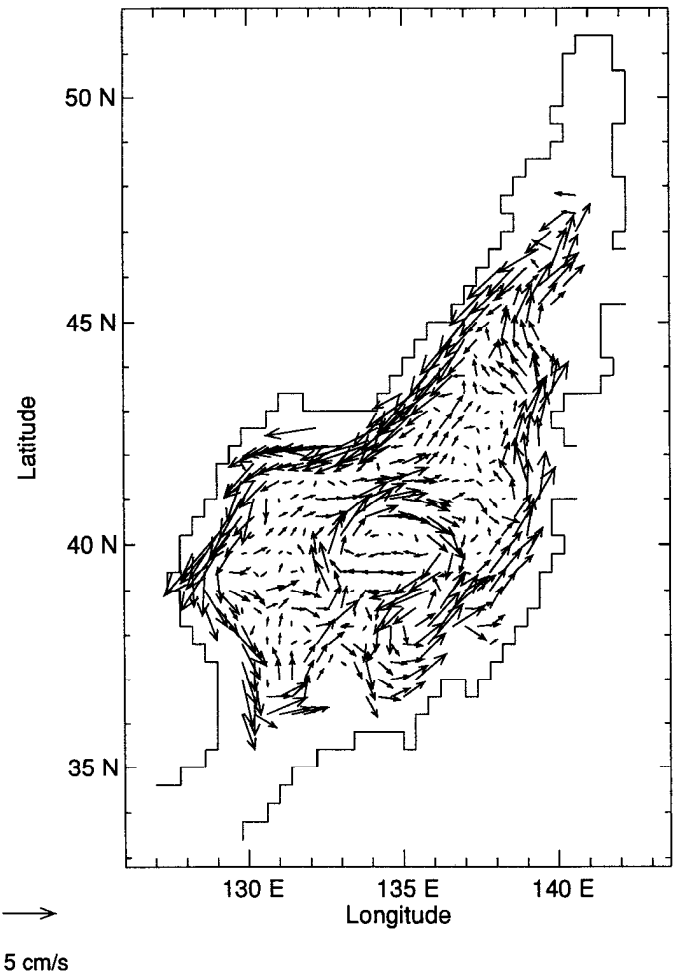

Figure 6h. L = 8 km at 720 m.

4) dependence upon internal parameters (as viscosity, diffusivity, and topostress),

5) dependence upon numerical aspects (as method for advection, timestep acceleration).

Although a thorough investigation of all of these dependences is beyond the scope of the present research, we offer some brief remarks below.

We considered cases in which surface forcing of heat and freshwater are implied by restoring surface layer T and S toward a reference climatology (Levitus). Thus heat and freshwater fluxes are not prescribed but rather evolve in response to the model state. Comparing restoring time-scales of 5, 20, 30, 60, 120, 240, 360, and 480 days with a control case (10 days) we found that quasi-periodic vacillations

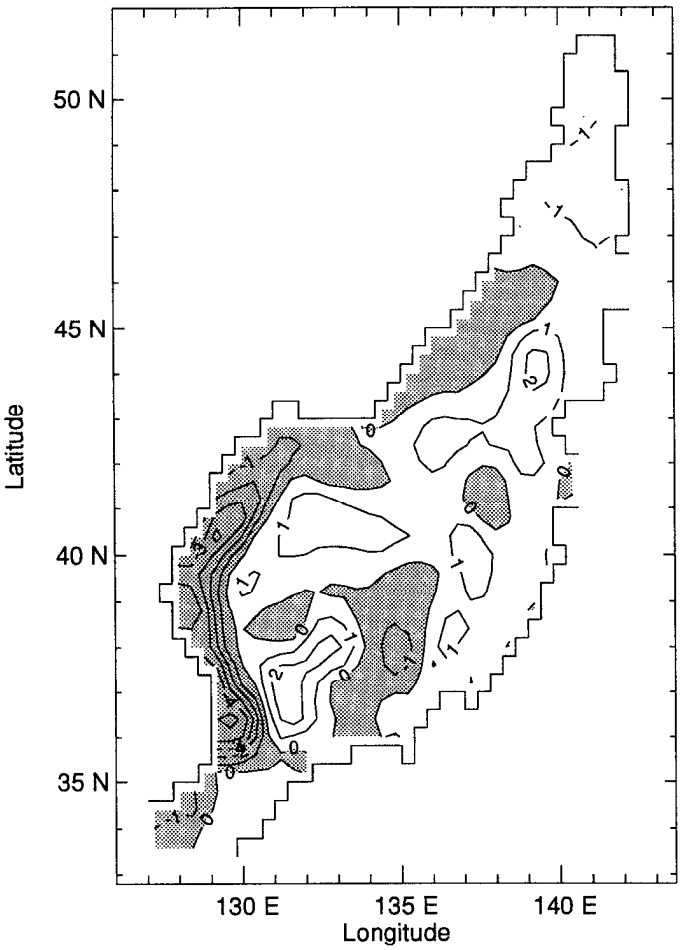

Figure 7. Difference fields from case L = 6 km minus L = 0 at 100 m for (a) potential temperature and (b) salinity.

persisted for all choices, though with somewhat diminished amplitude under long restoring times.

Previous studies by Marotzke *et al.* (1988), Weaver and Sarachik (1991), Power and Kleeman (1993), and Tziperman *et al.* (1994) show that models are sensitive to a mix of assigned and restoring fluxes for surface T and S. The restored flux condition was replaced with assigned fluxes, as well as combinations of restored and assigned fluxes, where assigned fluxes were derived under restoring conditions, averaged over a 20 year time period. Interannual variability persisted qualitatively similarly to cases using restoring boundary conditions.

Different combinations of wind stress and surface forcing of T and S revealed the vacillations' sensitivity to each of these forcing. Restoring T dominates the vacilla-

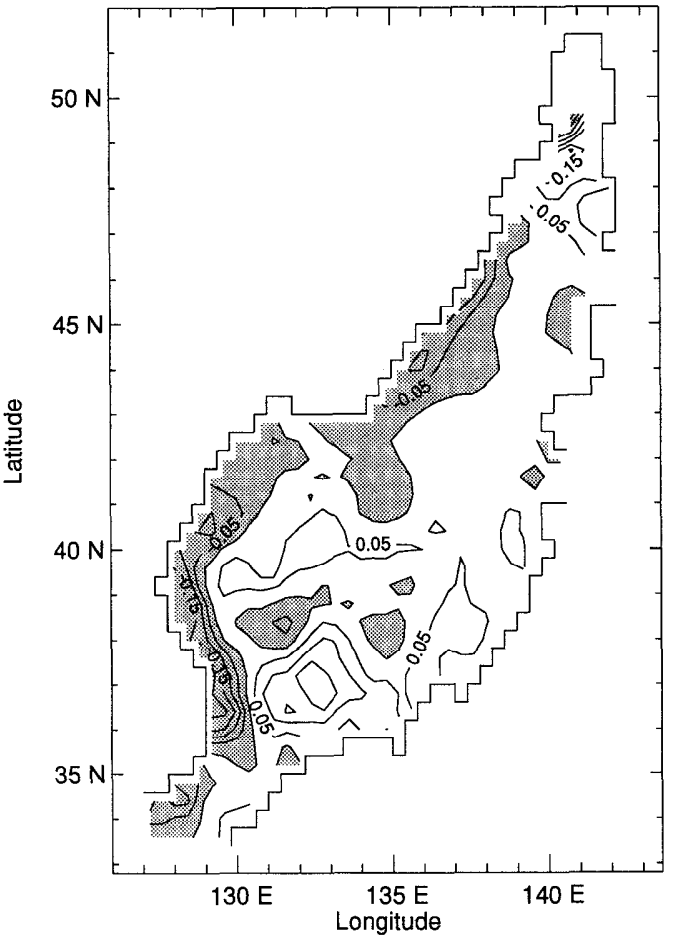

Figure 7. (Continued)

tion, while restoring S tends to be unimportant. Wind stress interacting with T contributes to the strength of vacillation.

Assigned steady inflow at Tsushima may play a substantial role. We assigned values 2.0, 0.75, 0.3 and zero Sv, to compare with control 1.5 Sv, while retaining the fractional discharge at Tsugaru and Soya Straits in proportions ¾ and ¼. Amplitude of variability was observed to decrease with decreasing inflow, yielding nearly steady flow for inflows of 0.3 Sv or less.

From Tsushima to Tsugaru straits, water gains roughly 10 degrees latitude and hence is subjected to significant change of planetary vorticity. To see how much this change contributes to internal variability we set the Coriolis parameter to a constant while wind, thermal, freshwater and throughflow forcing were as in the control case.

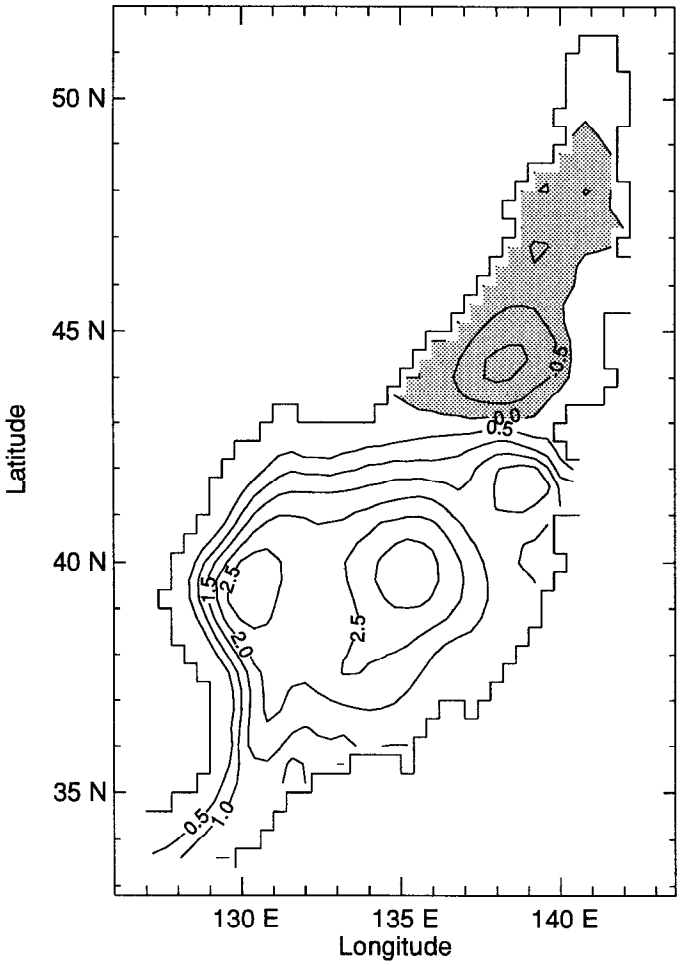

Figure 8. Transport streamfunction under steady forcing (a) in a minimum kinetic energy regime and (b) in a maximum kinetic energy regime.

The result was a substantial reduction in amplitude of vacillations, indicating that changes of planetary vorticity make significant contribution.

Various internal parameters were considered. Doubling the horizontal viscosity substantially reduced the vacillation in the seasonal case but had very little effect on the annual case. Disabling the model's convective adjustment had little effect. The topostress parameterization, while substantially affecting mean flow, had less effect on internal variability. Amplitude of vacillations is slightly increased with increased topostress parameter L.

Computational aspects also were considered. For economy, we employed "acceler-

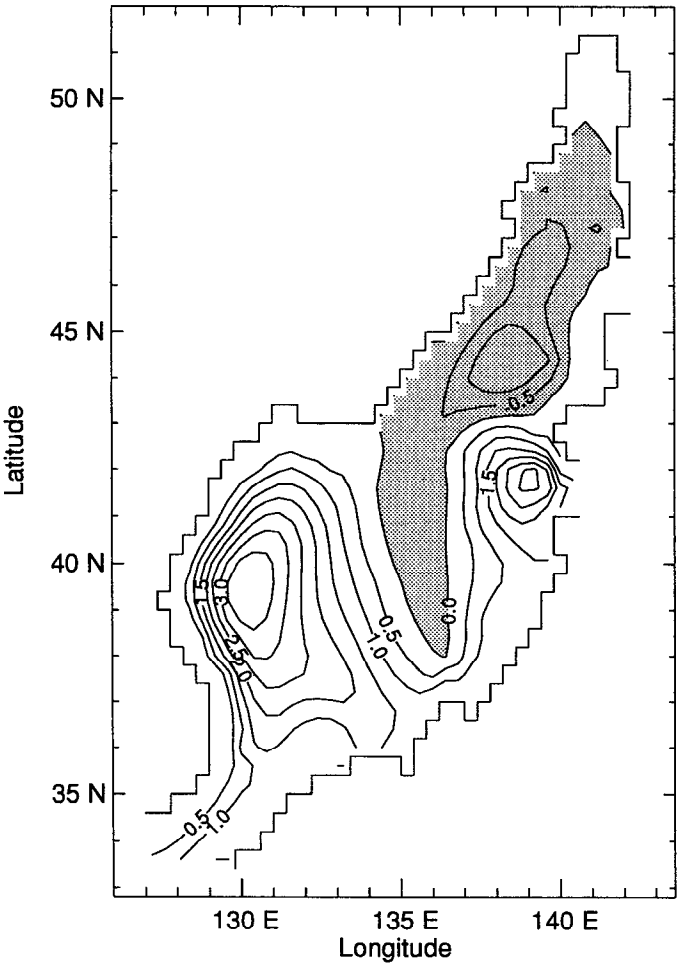

Figure 8. (Continued)

ated physics" following Bryan (1984) with a shorter timestep assigned in momentum equations while the system is timestepped on the longer tracer timestep. To study transient phenomena this is dangerous. We assessed the impact by comparing different acceleration ratios (tracer timestep: momentum timestep) from 36:1 to 1:1. Although qualitative character of the variability was not affected, the time-scales of variability showed dependence on the acceleration ratios. As well we compared FCT with centered difference advection without noting marked impact on the vacillations.

A striking observation is how effectively the imposition of a seasonal cycle on the forcing suppresses interannual variability. This is seen in Figure 9, showing time-series of the basin-integrated kinetic energy under both seasonal and steady forcing.

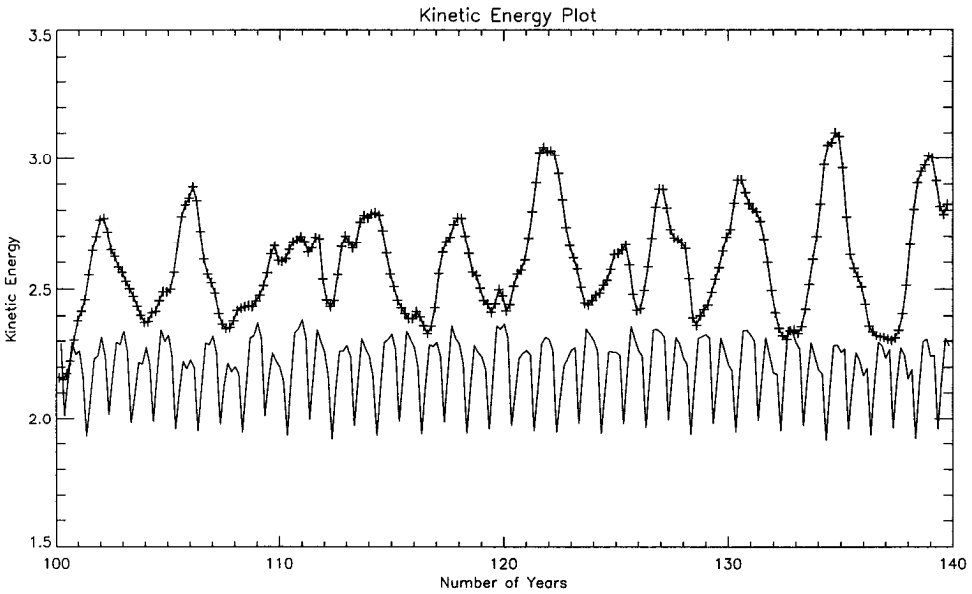

Figure 9. Basin-integrated kinetic energy under steady forcing (marked +) and seasonal forcing.

8. Summary

We have addressed a particular aspect of circulation dynamics, asking how much a statistical mechanical tendency arising from eddy-topography interaction can be incorporated into coarser resolution numerical models. Our aim has been not so much to make a "best" Japan Sea model (for which one would seek more accurate forcing datasets), but rather to identify shortcomings in underlying model physics. Results from a simple implementation show (1) that flow features can be significantly affected and (2) that apparent improvements can be made in areas that have frustrated earlier modelling. In particular, overshoot of the EKWC is reduced or eliminated and a strongly southward undercurrent brings colder, fresher water down along the Korean shelf. A stronger, more nearly continuous NB develops and the LC is strengthened. We obtain northward flow beneath the NB (where SK obtain a southward undercurrent), inviting observational testing.

We have explored sensitivity to poorly known eddy parameter L. Although "nice" results appear with L taking values of 4 or 6 km, one is cautioned that these values are likely corrupted to compensate for errors in forcing (wind, buoyancy, inflow), and dependence upon model resolution and other poorly known model parameters. We do see that traditional modelling ($L = 0$) exhibits clear defects under the external forcings we've considered. Most importantly we observe that model features, several of which have been previously remarked to be chronically defective, can be very

responsive to different L. Inclusion of topostress, hitherto absent in Japan Sea models, becomes a key concern.

We observed interannual variability under fixed (or perfectly repeating) external forcing and have performed experiments to identify significant factors in that variability. While the role of externally forced interannual variability should be an important consideration, we find that internally generated variability may be as large as observed variability. We find also that imposition of the seasonal cycle in forcing effectively suppresses the amplitude of low frequency fluctuations.

While progress is seen in some modelled circulation features, other systematic errors persist, for example in mean vertical distributions of heat (too warm at mid-depth) and salt (too fresh at mid-depth). These point to other errors, including poorly known thermal and freshwater forcing and (we suspect) inadequate model representation of convection.

Acknowledgments. This work was supported in part by the Office of Naval Research (N00014-92-J-1775).

REFERENCES

Alvarez, A., J. Tintore, G. Holloway, M. Eby and J. M. Beckers. 1994. Effect of topographic stress on the circulation in the western Mediterranean. J. Geophys. Res., *99,* 16,053–16,064.

Beckmann, A., C. W. Boning, C. Koberle and J. Willebrand. 1993. Effects of increased horizontal resolution in a simulation of the North Atlantic Ocean. J. Phys. Oceanogr., *24,* 326–344.

Bryan, F. O. and W. R. Holland. 1989. A high-resolution simulation of the wind- and thermohaline-driven circulation in the North Atlantic, *in* 'Aha Huliko'a Parameterization of Small Scale Processes', P. Muller and D. Henderson, eds., Hawaii Inst. of Geophysics, 99–115.

Bryan, K., 1969. A numerical method for the study of the circulation of the world ocean. J. Comput. Phys., *4,* 347–376.

—— 1984. Accelerating the convergence to equilibrium of ocean-climate models. J. Phys. Oceanogr., *14,* 666–673.

Cherniawsky, J. and G. Holloway. 1993. On western boundary current separation in an upper-ocean GCM of the North Pacific. J Geophys. Res., *98,* 22843–22853.

Eby, M. and G. Holloway. 1994a. Sensitivity of a large scale ocean model to a parameterization of topographic stress. J. Phys. Oceanogr., *24,* 2577–2588.

—— 1994b. Grid transform for incorporating the Arctic in a global ocean model. Climate Dyn., *10,* 241–247.

Ezer, T. and G. L. Mellor. 1992. A numerical study of the variability and the separation of the Gulf Stream, induced by surface atmospheric forcing and lateral boundary flows. J. Phys. Oceanogr., *22,* 660–682.

Gerdes, R., C. Koberle and J. Willebrand. 1991. The influence of numerical advection schemes on the results of ocean general circulation models. Climate Dyn., *5,* 211–226.

Hellerman, S. and M. Rosenstein. 1983. Normal monthly wind stress over the World Ocean with error estimates. J. Phys. Oceanogr., *13,* 1093–1104.

Holloway, G. 1992. "Representing topographic stress for large scale ocean models. J. Phys. Oceanogr., *22,* 1033–1046.

Ichiye, T., ed. 1984. Ocean Hydrodynamics of the Japan and East China Seas, Elsevier, 423 pp.

Kang, S. K., S. R. Lee and K.-D. Yum. 1991. Tidal computation of the East China Sea, the Yellow Sea and the East Sea," 25–48 in Takano (1991).

Kang, Y. Q. 1988. On the formation of the East Korean Warm Current. Ocean Res., *10,* 1–6.

Kawabe, M. 1982. Branching of the Tshushima Current in the Japan Sea. Part II. Numerical experiment. J. Oceaonogr. Soc. Japan, *38,* 183–192.

Kim, K., K.-R. Kim, J.-Y. Chung, H.-S. Yoo and S.-G. Park. 1991. Characteristics of physical properties in the Ulleung Basin. J. Oceanol. Soc. Korea, *26,* 83–100.

Levitus, S. 1982. Climatological Atlas of the World Ocean. NOAA Prof. Paper 13, Washington, D.C.

Lie, H.-J. and S.-K. Byun. 1985. Summertime southward current along the east coast of Korea. J. Oceanol. Soc. Korea, *20,* 22–27.

Lie, H.-J., M.-S. Suk and C. Kim. 1989. Observations of southeastward deep currents off the east coast of Korea. J. Oceanol. Soc. Korea, *24,* 63–68.

Marotzke, J., P. Welander and J. Willebrand. 1988. Instabilities and multiple steady states in a meridional-plane model of the thermohaline circulation. Tellus, *40A,* 162–172.

Na, J. Y., J. W. Seo and S. K. Han. 1992. Monthly mean seasurface winds over the adjacent seas of the Korean Peninsula. J. Oceanol. Soc. Korea, *27,* 1–10.

Nan-niti, T., H. Akamatsu and T. Yasuoka. 1966. A deep current measurement in the Japan Sea. The Oceanogr. Mag., *18,* 63–71.

Pacanowski, R., K. Dixon and A. Rosati. 1991. The GFDL Modular Ocean Model User's Guide Version 1.0, GFDL Ocean Group, Tech. Report No. 2, Princeton University, Princeton, NJ.

Power, S. B. and R. Kleeman. 1993. Multiple equilibria in a global ocean general circulation model. J. Phys. Oceanogr., *23,* 1670–1681.

Sekine, Y. 1986. Wind-driven circulation in the Japan Sea and its influence on the branching of the Tsushima Current. Progr. Oceanogr., *17,* 297–313.

—— 1991. A numerical experiment on the seasonal variation of the oceanic circulation in the Japan Sea. 113–128 in Takano (1991).

Seung, Y. H. 1992. A simple model for separation of East Korea Warm Current and formation of North Korea Cold Current. J. Oceanol. Soc. Korea, *27,* 189–196.

Seung, Y. H. and K. Kim. 1989. "On the possible role of local thermal forcing on the Japan Sea Circulation," J. Oceanol. Soc. Korea, *24,* 29–38.

—— 1993. A numerical modeling of the East Sea circulation. J. Oceanol. Soc. Korea, *28,* 292–304.

Takano, K., ed. 1991. Oceanography of Asian Marginal Seas, Elsevier, 431 pp.

Toba, Y., K. Tomizawa, Y. Kurasawa and K. Hanawa. 1982. Seasonal and year-to-year variability of the Tsushima-Tsugaru warm current system with its possible cause. La Mer, *20,* 41–51.

Tziperman, E., J. R. Toggweiler, Y. Feliks and K. Bryan. 1994. Instability of the thermohaline circulation with respect to mixed boundary conditions: Is it really a problem for realistic models? J. Phys. Oceanogr., *24,* 217–232.

Uda, M. 1935. The results of simultaneous oceanographical investigations in the North Pacific Ocean adjacent to Japan made in August 1933. J. Imp. Fish. Exp. Sta., *6,* 1–130.

Weaver, A. J. and E. S. Sarachick. 1991. The role of mixed boundary conditions in numerical models of the ocean's climate. J. Phys. Oceanogr., *21,* 1470–1493.

Yoon, J. H. 1982a. Numerical experiment on the circulation in the Japan Sea. Part I: Formation of the East Korea Warm Current. J. Oceanogr. Soc. Japan, *38,* 43–51.

—— 1982b. Numerical experiment on the circulation in the Japan Sea. Part II: Influence of seasonal variations in atmospheric conditions on the Tsushima Current. J. Oceanogr. Soc. Japan, *38,* 81–94.
—— 1982c. Numerical experiment on the circulation in the Japan Sea. Part III: Formation of the nearshore branch of the Tsushima Current. J. Oceanogr. Soc. Japan, *38,* 119–124.

Received: *14 November, 1994;* revised: *4 May, 1995.*